Lattice QCD at finite density via a new canonical approach

Andrei Alexandru,[1] Manfried Faber,[2] Ivan Horváth,[1] and Keh-Fei Liu[1]

[1]*Department of Physics and Astronomy, University of Kentucky, Lexington Kentucky 40506, USA*
[2]*Atomic Institute of the Austrian Universities, Nuclear Physics Division, A-1040 Vienna, Austria*

We carry out a finite density calculation based on a canonical approach which is designed to address the overlap problem. Two degenerate flavor simulations are performed using Wilson gauge action and Wilson fermions on 4^4 lattices, at temperatures close to the critical temperature $T_c \approx 170$ MeV and large densities (5 to 20 times nuclear matter density). In this region, we find that the algorithm works well. We compare our results with those from other approaches.

I. INTRODUCTION

The phase structure of QCD at finite temperature and finite density is relevant for a variety of phenomena: from subtle modifications of cross section in high energy collisions of nuclei, to exotic states of nuclear matter in neutron stars. Because of asymptotic freedom we can use perturbation theory to study the quark-gluon plasma at sufficiently large temperatures. However, the regions of interest for heavy ion collision experiments and astrophysics are essentially nonperturbative. Numerical studies of QCD are extremely helpful in providing a quantitative understanding of the phase structure in these regions.

At zero baryon density, it has been known for quite some time that QCD undergoes a transition from a confined phase to a deconfined phase at a temperature $T_c \approx 170$ MeV. Lattice QCD suggests that the transition is in fact a smooth crossover. This is expected to turn into a first order phase transition as the baryon density is increased. A schematic picture of the expected phase diagram is presented in Fig. 1.

The position of the second order transition point, where the crossover turns into a first order phase transition, is very important in providing a quantitative understanding of the QCD phase diagram. Close to the critical temperature the relevant degrees of freedom are the gluons and three flavors of quarks, the light quarks, up and down, and the strange quark. The shape of the curve seems to depend very little on the masses of the quarks, but the position of the second order transition point depends strongly on the mass of the strange quark. All numerical simulations treat the light quarks as degenerate. If the strange quark mass is taken to be equal to the mass of the light quarks, we have a theory with three degenerate flavors. In this case, for low enough quark masses, the zero density phase transition is expected to be first order, the second order point disappears. As the strange quark mass is increased, the zero density phase transition becomes a crossover, and the second order phase transition point moves to larger and larger densities. As the strange quark becomes infinitely heavy, only the light quarks remain dynamically relevant. The position of the second order phase transition point is not the same as in the

physically relevant case; however, qualitatively the picture remains the same. This is why two degenerate flavor QCD is interesting as a testbed for methods to simulate finite density QCD.

Simulations at finite temperature and zero baryon density can be performed using standard lattice techniques. However, nonzero baryon density calculations remain one of the challenges of Lattice QCD. The reason is that, at nonzero chemical potential, the fermionic determinant becomes complex and the standard Monte Carlo methods fail since the integrand is no longer real and positive definite. The usual approach is to split the integrand in two parts, one that is real and positive and can be employed to generate an ensemble of configurations, and another one that includes the complex phase of the determinant and is folded into the observables. For clarity, let us write the grand canonical partition function for Lattice QCD:

$$Z(V, T, \mu) = \int \mathcal{D}U \mathcal{D}\bar{\psi}\mathcal{D}\psi e^{-S_g(U) - S_f(\mu; U, \bar{\psi}, \psi)}, \quad (1)$$

The fermionic part of the action,
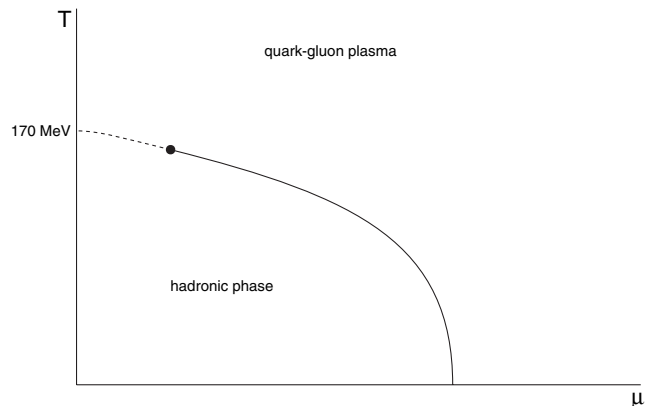
FIG. 1. Schematic picture of the expected QCD phase diagram. The solid line represents a first order phase transition, the dot a second order phase transition and the dashed line represents a crossover.

$$S_f(m, \mu; U, \bar{\psi}, \psi) = \bar{\psi}M(m, \mu; U)\psi, \qquad (2)$$

is a quark bilinear and we can perform the path integration analytically,

$$Z(V, T, \mu) = \int \mathcal{D}U e^{-S_g(U)} \prod_i \det M(m_i, \mu_i; U), \qquad (3)$$

where M is the quark matrix and m_i and μ_i are the mass and the chemical potential for flavor i. The gluonic part of the integrand, $e^{-S_g(U)}$, is real and positive, whereas the fermionic part is only guaranteed to be real when the chemical potential is zero. In the case of two degenerate flavors, after setting $\mu_1 = \mu_2 = \mu$, the partition function becomes

$$Z(V, T, \mu) = \int \mathcal{D}U e^{-S_g(U)} \det M(m, \mu; U)^2. \qquad (4)$$

The standard approach, the Glasgow reweighting method [1], is to split the fermionic part into a real positive part and a phase factor

$$\det M(\mu)^2 = \det M(\mu = 0)^2 \times \frac{\det M(\mu)^2}{\det M(\mu = 0)^2}, \qquad (5)$$

where we dropped some redundant indices. We can then apply the standard Monte Carlo techniques to generate an ensemble according to the measure,

$$P(U) = e^{-S_g(U)} \det M(\mu = 0)^2, \qquad (6)$$

and then insert the phase factor,

$$\theta(\mu; U) = \frac{\det M(\mu; U)^2}{\det M(\mu = 0; U)^2}, \qquad (7)$$

into the observable

$$\langle O(U) \rangle_\mu = \frac{\langle O(U)\theta(\mu; U) \rangle_{\mu=0}}{\langle \theta(\mu; U) \rangle_{\mu=0}}. \qquad (8)$$

To establish some terminology, we will call the ensemble generated with the weight $P(U)$ the *generated ensemble* and, in a manner of speaking, we will be calling *target ensemble* the one that would be generated using the weight derived from the true action. For the second term, the word ensemble is used loosely since for a complex integrand the concept of ensemble is, at best, ambiguous.

There are two major problems with the reweighting approach: the sign problem and the overlap problem. The sign problem appears when the phase factor, $\theta(\mu; U)$, averages to a value too close to zero on the generated ensemble. By close, we mean an average value that is smaller than the error. In that case, all the measurements will have sizable error bars and the method fails since we need extremely large ensembles to get reasonable error bars.

The second problem appears when the generated ensemble and the target ensemble overlap poorly; for example, they might be in different phases. More precisely, take an observable (in our example, the order parameter for the phase transition), if it happens that the histogram of this observable in the generated ensemble overlaps very poorly with the histogram in the target ensemble, then the value that we get via reweighting will be wrong. This problem is more serious than the sign problem since there is no indication when the measurement fails; the error bars can be deceptively small [1,2].

Recently, a lot of progress has been made in studying the phase diagram at temperatures around T_c and small chemical potential [3–7]. The reason is that, in this region, the sign problem is manageable and the overlap problem is expected to be under control. The methods employ a more or less sophisticated form of reweighting [3–6] or some form of analytical continuation from imaginary chemical potential [7]. The main results are the shape of the phase transition curve around T_c and the location of the second order phase transition point for quark masses close to the physical masses. All these simulations seem to be free of the sign problem, but it is not clear whether the overlap problem is indeed under control. One way to make sure that the results are correct is to either use methods that are proved to be free of overlap problem, or methods that are different enough but produce the same results. For small values of $\mu/T_c \ll 1$, different methods seem to agree. However, there is only one result for the location of the second order phase transition point, and it occurs at rather large value of the chemical potential. It is thus important to ask whether this result is reliable.

In light of the problems mentioned above, it is imperative that new methods be developed to simulate QCD at finite density. All the methods mentioned above are based on the grand canonical partition function. Far fewer attempts have been made to simulate QCD using the canonical partition function [8–10]. In this paper, we will present simulations based on a method that employs the canonical partition function [11–13]. The main idea is that, to avoid the overlap problem, it is essential to generate an ensemble that is based on the projected determinant, instead of reweighting. Moreover, to reduce the determinant fluctuations, the updating process is broken into two steps: an HMC proposal and an accept/reject step based on determinant ratios. These runs are exploratory in nature, using very small lattices and rather large quark masses. The main goal is to determine the feasibility of the algorithm and explore the available phase space.

The paper is organized as follows: in Sec. II we will introduce the canonical ensemble for QCD, in Sec. III we present the algorithm we employed, in Sec. IV we discuss the performance of the algorithm and in Sec. V we present the physical results. We then conclude by attempting a physical interpretation of our results in Sec. VI.

II. CANONICAL PARTITION FUNCTION

The simplest way to show how to build the canonical ensemble in Lattice QCD is to start from the fugacity expansion,

$$Z(V, T, \mu) = \sum_n Z_C(V, T, n)e^{\mu n/T}, \qquad (9)$$

where n is the net number of quarks (number of quarks minus the number of antiquarks) and Z_C is the canonical partition function. We note here that on a finite lattice, the maximum net number of quarks is limited by the Pauli exclusion principle. On a lattice of finite volume, using the fugacity expansion, it is easy to see that we can write the canonical partition function as a Fourier transform of the grand canonical partition function,

$$Z_C(V, T, n) = \frac{1}{2\pi} \int_0^{2\pi} d\phi e^{-in\phi} Z(V, T, \mu)|_{\mu=i\phi T}. \quad (10)$$

The result above was derived under the assumption that the partition function is analytical, which is true on a finite lattice. In the thermodynamic limit this is no longer true, however, the grand canonical and the canonical approaches are expected to produce the same results [9].

We will now specialize to the case of two degenerate flavors. We use the grand canonical partition function in Eq. (4) to get

$$Z_C(V, T, n) = \int \mathcal{D}U e^{-S_g(U)} \det_n M^2(U), \qquad (11)$$

where we define

$$\det{}_n M^2(U) \equiv \frac{1}{2\pi} \int_0^{2\pi} d\phi e^{-in\phi} \det M(m, \mu; U)^2|_{\mu=i\phi T}. \tag{12}$$

It is worth pointing out that the canonical partition function defined above sums over configurations where the total net number of quarks, $n = n_1 + n_2$, is fixed. If we want to fix the net quark number for each flavor then we would use $\det_{n_1} M(U) \times \det_{n_2} M(U)$.

For our study, we will be using Wilson fermions. To introduce a nonzero chemical potential, the fermion matrix at zero chemical potential,

$$[M(U)]_{x,y} = \delta_{x,y} - \kappa \sum_{\mu=1}^4 (1 - \gamma_\mu) U_\mu(x) \delta_{x+\hat{\mu},y}$$

$$- \kappa \sum_{\mu=1}^4 (1 + \gamma_\mu) U_\mu^\dagger(y) \delta_{x,y+\hat{\mu}}, \qquad (13)$$

is altered [14] by introducing a bias for time forward propagation in the hopping matrix. More specifically, the hopping in the time direction is altered

$$(1 + \gamma_4) U_4^\dagger(y) \rightarrow (1 + \gamma_4) U_4^\dagger(y) e^{\mu a},$$
$$(1 - \gamma_4) U_4(x) \rightarrow (1 - \gamma_4) U_4(x) e^{-\mu a}. \tag{14}$$

We can perform a change of variables [8],

$$\psi(\vec{x}, x_4) \rightarrow \psi'(\vec{x}, x_4) = e^{-\mu a x_4} \psi(\vec{x}, x_4),$$
$$\bar{\psi}(\vec{x}, x_4) \rightarrow \bar{\psi}'(\vec{x}, x_4) = e^{\mu a x_4} \bar{\psi}(\vec{x}, x_4) \tag{15}$$

to restore the original form of the hopping matrix except on the last time slice. In terms of these new variables, we can write the fermionic matrix as $M(U_\phi) = M(m, \mu; U)$ where M is defined in Eq. (13) and

$$(U_\phi)_\nu(x) \equiv \begin{cases} U_\nu(x)e^{-i\phi} & x_4 = N_t, \quad \nu = 4 \\ U_\nu(x) & \text{otherwise.} \end{cases} \tag{16}$$

This should not be viewed as a change of the gauge field variables but rather as a convenient way to write the fermionic matrix.

In order to evaluate numerically the partition function in Eq. (11), we need to replace the continuous Fourier transform in Eq. (12) with a discrete one. We will then redefine the projected determinant,

$$\widetilde{\det}{}_n M^2(U) \equiv \frac{1}{N} \sum_{j=0}^{N-1} e^{-in\phi_j} \det M(U_{\phi_j})^2. \tag{17}$$

where $\phi_j = \frac{2\pi j}{N}$ and the parameter N defines the discrete Fourier transform. In the limit $N \rightarrow \infty$, we recover the original projected determinant. For finite N the partition function

$$\tilde{Z}_C(V, T, n) \equiv \int \mathcal{D}U e^{-S_g(U)} \widetilde{\det}{}_n M^2(U), \tag{18}$$

will only be an approximation of the canonical partition function. Using the fugacity expansion we can show that

$$\tilde{Z}_C(V, T, n) = \sum_{m=-\infty}^{\infty} Z_C(V, T, n + mN). \tag{19}$$

If N and n are chosen such that $|n + mN|$ is minimal for $m = 0$ then $\tilde{Z}_C$ should be a good approximation to Z_C as long as

$$\frac{Z_C(V, T, n + mN)}{Z_C(V, T, n)} \ll 1, \tag{20}$$

for all $m \neq 0$. To understand better this condition take $0 \leq n < N/2$; the largest contamination comes from $Z_C(V, T, N - n)$. The ratio above is

$$\frac{Z_C(V, T, N - n)}{Z_C(V, T, n)} = e^{-[(F(V,T,N-n)-F(V,T,n))/T]}, \tag{21}$$

where F is the free energy of the system. For low temperatures, we expect that $F(V, T, n) \propto e^{-M_B |n|/3}$, where M_B is the mass of the baryon. We see then that the approximation will hold as long as the temperature is low enough or the

baryon mass is high. This assumption needs to be checked in our simulations; if it fails then we need to increase N.

III. ALGORITHM

In this section, we will present the algorithm we employ to simulate the partition function $\tilde{Z}_C$. Directly simulating the projected determinant in Eq. (17) is known to face a fluctuation problem [15], since $\ln \det M = \mathrm{Tr}\ln M$ and $\mathrm{Tr}\ln M$ is proportional to the lattice volume. To alleviate the problem we split the Markov process in two steps: a proposal step based on HMC and an accept/reject step based on the ratio of the projected determinant to the determinant used in the HMC step. Since the accept/reject is based on the determinant ratio, the fluctuations should be reduced and the acceptance rate enhanced. We shall test this numerically.

A. Target measure

To evaluate $\tilde{Z}_C$ using Monte Carlo techniques, we need the integrand to be real and positive. Using γ_5 hermiticity of the fermionic matrix, i.e.

$$\gamma_5 M(U_\phi)\gamma_5 = M(U_\phi)^\dagger, \qquad (22)$$

we can easily prove that $\det M(U_\phi)$ is real. This implies that

$$\widetilde{\det}_n M^2(U) = (\widetilde{\det}_{-n} M^2(U))^*, \qquad (23)$$

but it does not imply that the projected determinant is real. $\widetilde{\det}_n M^2(U)$ is real only if $\det M(U_\phi) = \det M(U_{-\phi})$, which is not true configuration by configuration. We can prove that for a charge conjugation symmetric action, this property is true when averaged over the ensemble, i.e. $\langle \det M(U_\phi)\rangle = \langle \det M(U_{-\phi})\rangle$. In fact, using charge conjugation symmetry of the action, we can prove that

$$\tilde{Z}_C(V, T, n) = \tilde{Z}_C(V, T, -n). \qquad (24)$$

This property allows us to rewrite the partition function

$$\tilde{Z}_C(V, T, n) = \int \mathcal{D}U e^{-S_g(U)} \mathrm{Re}\widetilde{\det}_n M^2(U). \qquad (25)$$

Now the integrand is real but not necessarily positive. For the sake of the argument, let us set aside for a while the fact that the integrand may be negative and assume that the above expression can be evaluated using standard Monte Carlo techniques. Even then, the fact that we can write the partition function using a real integrand is not sufficient. The goal of any simulation is to compute different observables, the partition function itself is not of much interest. If we are only interested in observables that are even under charge conjugation, then we could use the ensemble generated by the above action to compute them. For observables that are odd under charge conjugation an additional step is necessary: we have to reintroduce a phase.

We want to emphasize that, if the above integrand is positive, the observables which are even under charge conjugation could be evaluated directly on the ensemble generated by the above action. Thus, we would have no reweighting involved, and no overlap problem. The observables that are odd under charge conjugation are not guaranteed to behave as well, but we assume that their behavior would be similar. At the worst, the extra phase might introduce a sign problem.

We come back now to the positivity question. In the case that the integrand is not positive, we are forced to use the absolute value of the integrand as measure for our generated ensemble. The algorithm will then be designed to generate an ensemble according to the weight

$$W(U) = e^{-S_g(U)}|\mathrm{Re}\widetilde{\det}_n M^2(U)|. \qquad (26)$$

The sign will be folded into the observables. For a generic observable the sign will turn out to be some complex phase,

$$\alpha(U) = \frac{\widetilde{\det}_n M^2(U)}{|\mathrm{Re}\widetilde{\det}_n M^2(U)|}, \qquad (27)$$

but for observables even under charge conjugation it will be just the sign of $\mathrm{Re}\widetilde{\det}_n M^2(U)$.

From the above discussion, it is clear that as long as we do not have a sign problem, the results of our simulation for observables invariant under charge conjugation are reliable. For the other observables, the sign problem might be more severe, but we expect that they will not have an overlap problem.

B. HMC update

Turning to the algorithmic issues, our approach to generating an ensemble with weight $W(U)$ is to employ a Metropolis accept/reject method. In short, the method employs a generating mechanism that proposes new configurations with weight $W'(U)$ and then an accept/reject step is used to correct for the target weight. Ideally, the proposal mechanism would propose configurations with the weight $W(U)$; in that case all new proposals will be accepted. In practice, it is not always possible to design efficient proposal mechanism for every weight. The general approach is to use an efficient proposal mechanism to generate a weight $W'(U)$ close to the target weight $W(U)$. If successful, the acceptance rate would be high and the algorithm would be efficient.

One possible solution is to use a heat-bath method to propose new configurations based on the weight $W'(U) = e^{-S_g(U)}$. However, such an updating strategy would be inefficient since the fermionic part is completely disregarded in the proposal step. The determinant, being an extensive quantity, can fluctuate wildly from one configuration to the next in the pure gauge updating process [15,16]. To reduce the fluctuations, it was suggested [12]
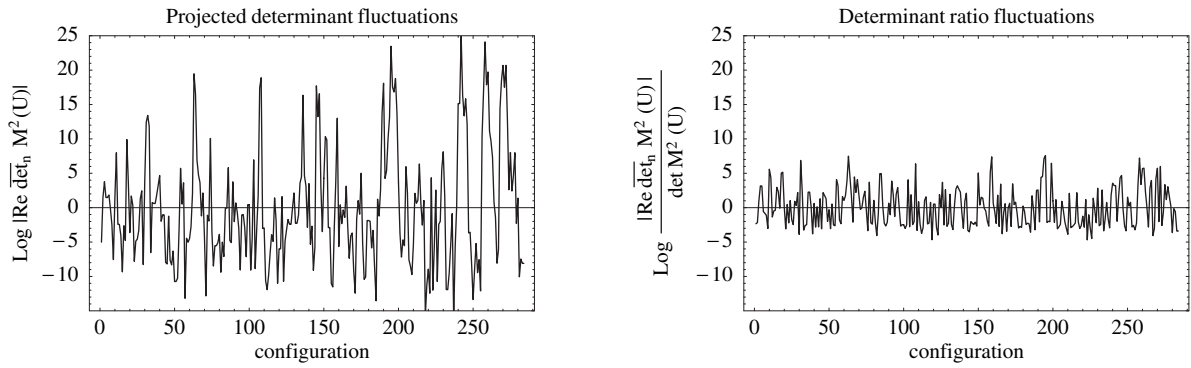
FIG. 2. Fluctuations of the fermionic part of the measure and of the accept/reject factor $\omega(U)$, defined in Eq. (30), as measured on an ensemble generated at $\beta = 5.2$ and $n = 3$. In both figures, we subtracted the average value so that the plots are centered around zero.

that we should employ an HMC algorithm for the proposal step. In this case

$$W'(U) = e^{-S_g(U)} \det M(U)^2. \quad (28)$$

We will then accept the new configuration U' with the probability

$$P_{acc} = \min\{1, \omega(U')/\omega(U)\}, \quad (29)$$

where ω is the ratio of the weights

$$\omega(U) = \frac{W(U)}{W'(U)} = \frac{|\text{Re}\widetilde{\det}_n M^2(U)|}{\det M^2(U)}. \quad (30)$$

We expect that this proposal mechanism will be more efficient. Although the fermionic part of the measure $|\text{Re}\widetilde{\det}_n M^2(U)|$ varies significantly from one configuration to the next, the determinant ratio

$$\omega(U) = \frac{1}{N} |\sum_{j=0}^{N-1} \cos(\phi_j n) e^{\text{Tr}(\log M(U_{\phi_j}) - \log M(U))}| \quad (31)$$

is expected to fluctuate less. We base our expectation on the fact that, in the ratio, the leading fluctuations are removed by the Tr log difference of the quark matrices $M(U_{\phi_j})$ and $M(U)$. To check this, we compare the fluctuations in the fermionic part of the determinant and the determinant ratios in one of the ensembles generated in our runs. This is shown in Fig. 2. We see that the fluctuations are significantly reduced which results in a large boost in acceptance rate.

C. Triality

The canonical partition function, Eq. (11), has a Z_3 symmetry [17] that is a direct consequence of the Z_3 symmetry of the grand canonical partition function at imaginary chemical potential [18]. Under a transformation $U \rightarrow U_\phi$ with $\phi = \pm 2\pi/3$, the gauge part of the action is invariant and

$$\det{}_n M^2(U) \rightarrow \det{}_n M^2(U_{\pm 2\pi/3}) = e^{\pm i[(2\pi)/3]n}\det{}_n M^2(U). \quad (32)$$

We see then that when n is a multiple of 3 this transformation leaves $\det_n M^2(U)$ invariant. Consequently, the canonical partition action is invariant under this transformation. Incidentally, this symmetry of the gauge part of the action together with the transformation above of the fermionic part guarantees that the canonical partition function will vanish when n is not a multiple of 3. However, this is no longer true if this symmetry is spontaneously broken, which is the case in the deconfined phase. In this phase, there is no reason to expect that the canonical partition function should vanish when n is not a multiple of 3.

The transformation rule above is preserved for the discrete case if we choose N, the parameter that defines the Fourier transform, to be a multiple of 3. In our simulations, we will always choose N to satisfy this condition. In this case, the remarks we made about Z_C are valid for $\tilde{Z}_C$ and the projected determinant, $\widetilde{\det}_n M^2(U)$ is invariant. Thus, the measure is symmetric under this transformation, i.e.

$$W(U) = W(U_{\pm 2\pi/3}). \quad (33)$$

However, the HMC weight, $W'(U)$, does not have this symmetry since $\det M(U)$ is not invariant under this transformation. Because of this, our algorithm can become frozen for long periods of time. For example, in Fig. 3, we show how the argument of the Polyakov loop changes with the simulation time if we use the method presented so far. We notice that at the end of the simulation, when we tunnel to the sector where $\arg[P] \approx 2\pi/3$, the update is frozen; the new proposals are rejected for a long time. This is due to the fact that HMC strongly prefers the 0 sector. To understand this better, assume that we have a configuration U_0 in the 0 sector, where $\arg[P(U_0)] \approx 0$, and denote with U_+ the configuration $(U_0)_{2/3}$ with $\arg[P(U_+)] \approx 2\pi/3$. Then, we expect that $\det M^2(U_0) \gg \det M^2(U_+)$ since HMC prefers the 0 sector, but $\widetilde{\det}_n M^2(U_0) = \widetilde{\det}_n M^2(U_+)$ since the projected determinant is symmetric under the Z_3
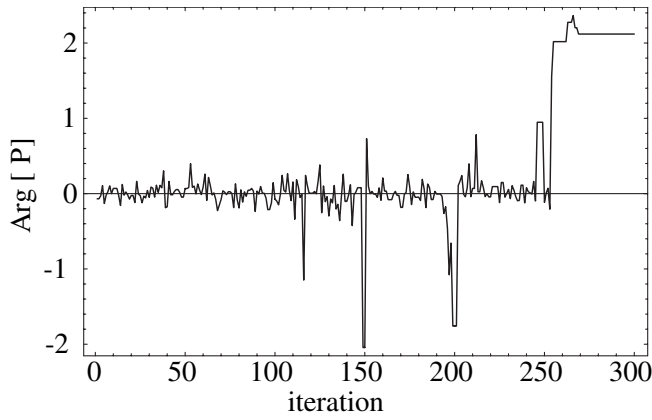
FIG. 3. Polyakov loop argument as a function of the simulation time. Note that toward the end the value is unchanged for almost 50 iterations.

transformations. Assume now that HMC proposes U_+, the accept/reject step will accept this since

$$\frac{\omega(U_+)}{\omega(U_0)} = \frac{\det M^2(U_0)}{\det M^2(U_+)} \gg 1. \qquad (34)$$

However, in the next step HMC is likely to propose a new configuration in the 0 sector since it favors it strongly. By the reverse of the argument above we have that

$$\frac{\omega(U_0)}{\omega(U_+)} = \frac{\det M^2(U_+)}{\det M^2(U_0)} \ll 1 \qquad (35)$$

and the new configuration will be very likely rejected.

This means that although the algorithm will end up sampling the three sectors equally, as required by the symmetric weight $W(U)$, two of the sectors will take a very long time to sample properly. To address this problem, we introduce a Z_3 hopping [9]. Since the weight $W(U)$ is symmetric under the Z_3 transformation, we can intermix the regular updates with a change in the field variables $U \to U_{\pm 2\pi/3}$. We will choose the sign randomly, with equal probability for each sign, to satisfy detailed balance. The new algorithm will sample all sectors in the same manner.

IV. SIMULATION DETAILS

Most of the computer time in these simulations is spent computing the determinant. There is a proposal that would employ a determinant estimator [19], but in this work we compute the determinant exactly using LU decomposition. This is a very expensive calculation considering that even for the small lattices we used in this study the fermionic matrix has 3 072 rows. Furthermore, the algorithm scales with the third power of the lattice four volume and it is not easily parallelizable. The high computational cost constrains us to use only 4^4 lattices for this study.

TABLE I. Simulation parameters.

β	a(fm)	m_π(MeV)	V^{-1}(fm^{-3})	T(MeV)
5.00	0.343(2)	926(7)	0.387(7)	144(1)
5.10	0.322(4)	945(13)	0.468(17)	153(2)
5.15	0.313(3)	942(11)	0.510(15)	157(2)
5.20	0.300(1)	945(5)	0.579(6)	164(1)
5.25	0.284(5)	945(20)	0.682(36)	173(3)
5.30	0.260(1)	973(9)	0.889(10)	189(1)
5.35	0.233(2)	959(14)	1.235(32)	211(2)

The computational cost increases linearly with the parameter N used to define the Fourier transform. For our study, we used $N = 12$. For each value of β we run three simulations: $n = 0$, $n = 3$, and $n = 6$. They correspond to 0, 1, and 2 baryons in the box.

Since our volume in lattice units is small, we had to use large lattice spacings. We had runs for $\beta = 5.00$, 5.10, 5.15, 5.20, 5.25, 5.30, and 5.35 and we fixed $\kappa = 0.158$. The relevant parameters can be found in Table I. The lattice spacing and the pion mass are determined using standard dynamical action on a 12^4 lattice for the same values of β and κ. The lattice spacing was determined by using r_0 scale [20]. We note that the pion mass varies very little with β, consequently the quark mass is roughly the same in all runs. We also note that the quark mass is quite heavy, above the strange quark mass.

For the HMC update, we used the Φ algorithm [21] made exact by an accept/reject step at the end of each trajectory [22]. For updating process, we set the length of the trajectories to 0.5 with $\Delta\tau = 0.01$. The HMC acceptance rate was very close to 1 since the step length was very small. We adjust the number of HMC trajectories between two consecutive finite density accept/reject steps so that the acceptance rate stays in the range 15% to 30%. The relevant information is collected in Table II. From the table we see that as we decrease β the acceptance rate drops. Since both volume and temperature are changed when we vary β it is not clear which parameter is responsible for the acceptance rate drop. To address this question, we need to run a simulation on a lattice with different volume.

TABLE II. Acceptance rates; we list first the number of HMC trajectories between two consecutive finite density Metropolis steps and then the acceptance rate.

β	HMC traj	$n = 0$	HMC traj	$n = 3$	HMC traj	$n = 6$
5.00	50	0.59(2)	20	0.27(1)	02	0.19(1)
5.10	50	0.55(2)	20	0.29(2)	05	0.15(1)
5.15	50	0.53(1)	20	0.25(2)	05	0.18(1)
5.20	50	0.49(2)	20	0.26(2)	05	0.25(2)
5.25	50	0.40(2)	20	0.32(1)	05	0.40(2)
5.30	50	0.36(1)	50	0.34(2)	10	0.32(2)
5.35	50	0.33(2)	50	0.34(2)	10	0.38(1)

However, increasing the lattice volume is not feasible with the current setup. We plan to answer this question in a future study. While this decrease in acceptance rate limits our ability to explore the low temperature region, we see that for the range of parameters studied in this paper we get decent acceptance rates even when consecutive finite density Metropolis steps are quite far apart in configuration space. To better quantify this statement we need to measure the autocorrelation time. Unfortunately, autocorrelation is very hard to measure since it requires very large statistics. To get an estimate of the autocorrelation time, we ran a long pure HMC simulation for a 4^4 lattice at $\beta = 5.10$ and $\kappa = 0.158$. The measured autocorrelation time for the plaquette is $\tau_{\mathrm{auto}} = 11.5(1.5)$ in units of trajectories of length 0.5. Adjusting this autocorrelation time for the acceptance rate and the number of trajectories between two successive finite density accept/reject steps we get $\tau_{\mathrm{auto}} = 0.4$, 2.0, and 15.3 for $n = 0$, 3 and 6, respectively, in units of time between two finite density accept/reject steps. Since we are saving configurations separated by 10 such steps we see that for $n = 0$ and 3 the configurations are independent, whereas for $n = 6$ they are correlated. However, since we use binned jackknife to estimate our error bars we do not expect this correlation to affect our results. We collected about 100 configurations for each run.

From an algorithmic point of view, one of the most interesting questions is whether or not we have a sign problem. To settle this question, we measured the average phase $\alpha(U)$ given in Eq. (27). In fact, it is easy to prove that the imaginary part of the phase should vanish on the ensemble average. It is the real part of this phase that carries the signal of a sign problem; if its average is close to zero then we have a sign problem. We note here that the real part of the phase is ± 1, and that the sign problem appears when we have an almost equal number of configurations of each sign.

In Fig. 4, we plot the average of the real part of the phase α as a function of the temperature. We note that in the deconfined phase, the projected determinant is positive most of the time; as we go into the hadronic phase the sign starts oscillating. Deep in the hadronic phase, the oscillations are more severe at higher density which we can see by comparing the case of $n = 6$ with $n = 3$ in Fig. 4. However, it is possible that at $T < T_c$ the sign average is actually smaller at lower density. This is due to the fact that, at this temperature, it is possible to have the system in the hadronic phase at low densities and in the quark-gluon plasma phase at higher densities. Since the oscillations are more severe in the hadronic phase it is not surprising that close to and below T_c we would have more sign oscillations at lower density. This could explain the average sign reversal of $n = 3$ and $n = 6$ at $T = 164$ MeV as compared to those at other temperatures in Fig. 4.

In Fig. 4, we also see that the sign average drops sharply as we go through the transition temperature but the rate
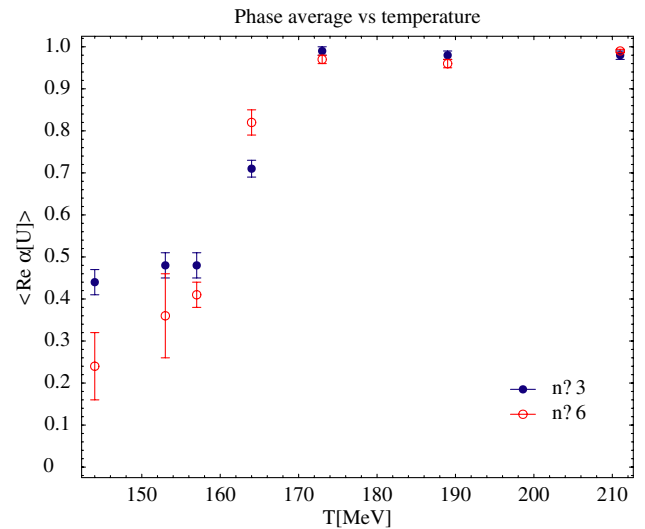
FIG. 4 (color online). Average phase for $n = 3$ and $n = 6$ runs. The $n = 0$ runs have all signs equal to 1 so we did not plot them in this figure.

slows down, as we go deeper in the hadronic phase. This slowing down may be due to the fact that as we go to lower and lower temperatures, the physical volume of the box is also increased and the density decreases.

Before concluding we would like to point out that the sign dependence on temperature and density is similar with the one observed in studies that employ the grand canonical partition function [6,23].

In conclusion, it seems that, at least for a 4^4 lattice, we have been able to investigate the region where $T > 0.8T_c$ and baryon number $n_B < 3$. From Table I we see that the densities used in this study are rather large; they range from 2.4 to 24 times the nuclear matter density. An interesting future direction would be to increase the spatial volume, using, for example, a $6^3 \times 4$ lattice, while keeping the baryon number the same. This would allow us to study densities closer to the physically interesting region. We should point out that it is possible that the sign problem would prevent us from increasing the volume; a simple argument seems to suggest that the sign oscillations are proportional to the volume. However, it is speculated [10] that the sign oscillations are mainly determined by the baryon number rather than the volume. If this is the case, we should be able to use our algorithm to explore this region. The dependence of the sign problem on volume is one of the questions we are planning to study in our future simulations. It is also clear that a sign problem will appear at baryon numbers larger than the ones employed in this study. We have also shown that the algorithm can be efficient in going through the configuration space. However, for nonzero density runs, the acceptance rate drops quite significantly with the temperature; much smaller number of trajectories have to be used between the successive accept/reject steps. This may be due to a

decrease in the autocorrelation time; as we go to smaller values of β the autocorrelation is expected to decrease. A more detailed study is needed to quantify this statement.

V. PHYSICAL RESULTS

We turn now toward the physical results. We will present measurements of the Polyakov loop, chemical potential, chiral condensate and the conserved charge. We feel compelled to point out that the results presented here have large systematic errors. The lattice volume and the baryon number are small, consequently the finite size effects are going to be important. The lattice spacing is very large and the lattice artifacts will be substantial. Since we are using Wilson fermions we expect that the chiral symmetry is broken quite badly by lattice terms. Also, the quark mass is rather heavy. In light of these problems, the results presented in this section are interesting more as proof of concept results.

A. Polyakov loop

The most straightforward way to look for a deconfining transition is to measure the Polyakov loop. Unlike the grand canonical approach, the action of the canonical partition function has a $Z(3)$ symmetry [17]. Although the average value is expected to vanish due to this Z_3 symmetry, we can look at the average absolute value. This is expected to increase sharply as we go from the confined to the deconfined phase. To measure the Polyakov loop we need to fold in the phase

$$\langle |P| \rangle = \frac{\langle |P|\alpha\rangle_0}{\langle \alpha\rangle_0}, \qquad (36)$$

where we denoted with $\langle\rangle_0$ the average over generated
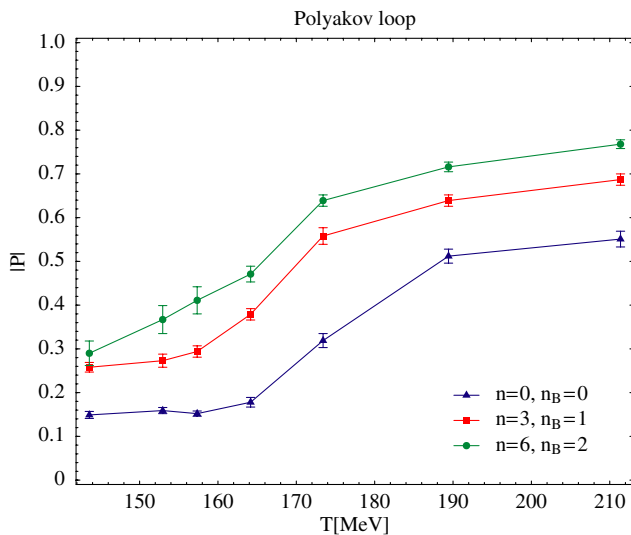
FIG. 5 (color online). Polyakov loop as a function of temperature.
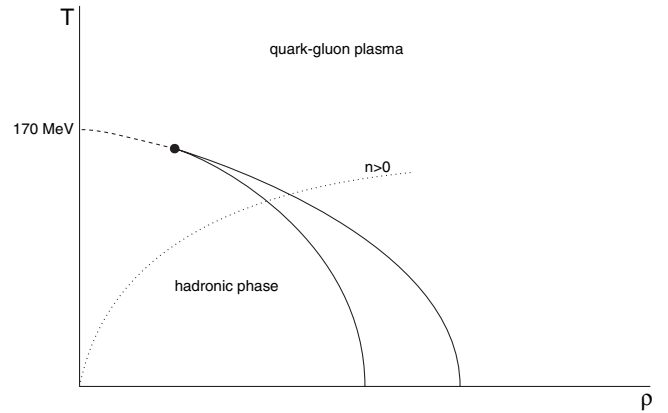
FIG. 6. A schematic view of the expected QCD phase diagram in the temperature-density plane [8]. The dotted line, $n > 0$, represents the trajectory in the phase space when we keep the baryon number fixed and vary β.

ensemble. In Fig. 5, we plot the Polyakov loop for our three sets of simulations as a function of temperature. We see that a transition occurs somewhere around 170 MeV for zero density and, as we increase the density, the transition becomes less sharp and moves to lower temperature. This picture agrees with the expectations from a study with static quarks [8], since at large densities the transition is expected to be first order and, as a result, the system will develop a coexistence region. To visualize this, we plot in Fig. 6 the expected phase diagram in the temperature-density plane. The main difference from the picture in the temperature - chemical potential plane (see Fig. 1) is that the first order transition line is split; we have now a line that borders the pure hadronic phase and another that borders the pure quark-gluon plasma phase. In between them, we have a coexistence region characteristic of a first order phase transition. As we go through this region, we expect a more pronounced slope in $|P|$. In the infinite volume limit, we expect that the slope will change abruptly as we go through the phase boundaries but we will not see an abrupt jump in our finite density study.

B. Chemical potential

In order to compare our results with the results in the grand canonical ensemble, we need to measure the chemical potential. The thermodynamic definition

$$\mu(n) = \frac{\partial F(V,T,n)}{\partial n} = -\frac{1}{\beta}\frac{\partial \ln\tilde{Z}_C(V,T,n)}{\partial n} \qquad (37)$$

would produce

$$\beta\mu(n) = i\frac{1}{\tilde{Z}_C(V,T,n)}\int \mathcal{D}U e^{-S_g(U)} \times \frac{1}{N}$$

$$\times \sum_{j=0}^{N-1} \phi_j e^{-in\phi_j} \det M^2(U_{\phi_j}) = \langle i\phi\rangle_n, \qquad (38)$$

where $\beta = 1/k_B T$. There are a number of problems with this definition. Firstly, the partition function is symmetric under the transformation $\phi_j \rightarrow \phi_j + 2\pi$. This is not true for this definition of the chemical potential and then we can ask why would the chemical potential depend on our choice of ϕ_j. Secondly, the chemical potential defined above is the quark chemical potential; it measures the response of the system when one more quark is introduced in the system. If we follow the same logic and measure the baryon chemical potential we find that $\mu_B(n_B) = \langle i3\phi \rangle_{3n_B} = 3\mu(3n_B)$. Thus, it seems that the response to introducing a baryon in the system is linearly related to the quark chemical potential. While this might be true in the deconfined phase, it is clearly not so in the confined phase. The cost of introducing one quark in an empty box should be infinite, whereas we expect that the cost of introducing a baryon should be finite. To address these shortcomings, we "discretize" the derivative and define the chemical potential

$$\mu(n) = \frac{F(n + 1) - F(n)}{(n + 1) - n} = F(n + 1) - F(n). \quad (39)$$

We see that defined as above, the chemical potential measures the increase in the free energy as we add a quark to the system. We find then

$$\mu(n) = -\frac{1}{\beta} \ln \frac{\tilde{Z}_C(n + 1)}{\tilde{Z}_C(n)}$$
$$= -\frac{1}{\beta} \frac{1}{\tilde{Z}_C(n)} \int \mathcal{D}U e^{-S_g(U)}$$
$$\times \frac{1}{N} \sum_{j=0}^{N-1} e^{-i\phi_j} e^{-in\phi_j} \det M^2(U_{\phi_j})$$
$$= -\frac{1}{\beta} \langle e^{-i\phi} \rangle_n. \quad (40)$$

Similarly, for the baryon chemical potential we find

$$\mu_B(n_B) = -\frac{1}{\beta} \langle e^{-i3\phi} \rangle_{3n_B}. \quad (41)$$

With these new definitions, the quark and baryon chemical potentials are no longer linearly related and they also satisfy the same symmetries as the partition function. Moreover, since the partition function for a system with a number of quarks that is not a multiple of 3 vanishes when we are in the confined phase, we have

$$\mu(3n) = -\frac{1}{\beta} \ln \frac{\tilde{Z}_C(3n + 1)}{\tilde{Z}_C(3n)} = +\infty, \quad (42)$$

which is exactly what we expect.

We note that the chemical potential as defined above has certain symmetries; since we used $\tilde{Z}_C$ for our definitions we have:

$$\mu(n) = \mu(n + N), \qquad \mu_B(n_B) = \mu_B(n_B + N/3), \quad (43)$$

the second equality holds when N is a multiple of 3. From charge conjugation symmetry, we infer that for $n, n_B > 0$

$$\mu(-n) = -\mu(n - 1)\mu_B(-n_B) = -\mu_B(n_B - 1). \quad (44)$$

In Fig. 7, we plot the baryon chemical potential as a function of temperature. We see that, as we go through the phase transition, the chemical potential drops sharply. This is due to the fact that new degrees of freedom become available and the entropy of the system increases. We notice that in the confined phase, the chemical potential does not change much as we increase the density, whereas in the deconfined region the chemical potential is larger as the density increases. These findings are consistent with the results of Kratochvila and de Forcrand [9,10]. We would also like to point out that since in our simulations we used $N = 12$, we can show, using the symmetries of the chemical potential listed above, that $\mu_B(2) = -\mu_B(1)$. This is why we plot only the curves for $n_B = 0$ and $n_B = 1$.

Computing the chemical potential allows us not only to connect our results to those from grand canonical simulations, but also to determine the shape of the phase boundary. To see this, we follow an argument by Kratochvila and de Forcrand [10]. They start by noticing that the chemical potential in the hadronic phase seems independent of the baryon number. Based on this observation they build a simple model where the free energy is proportional to the baryon number, $F(n_B) = \mu_0 |n_B|$. The coefficient μ_0 is the value of the chemical potential measured; they show that in this model μ_0 is just the critical chemical potential. Consequently, at any temperature T if we find μ to be independent of n_B we have determined $\mu_c(T)$.

The argument above can be generalized. In a physical system, the chemical potential is expected to vary from small values at small densities to arbitrarily large values as
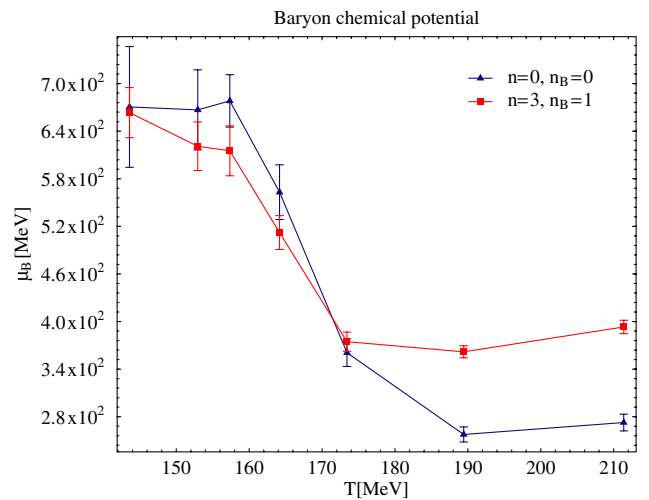
FIG. 7 (color online). Baryon chemical potential as a function of the temperature. We did not include the data for $n = 6$ since it replicates the results for $n = 3$.

the density goes to infinity. However, it can be argued on general grounds that when the chemical potential stays the same for a range of baryon numbers we are at a phase transition. In the thermodynamic limit, the free energy is a convex function of the baryon number and thus

$$\frac{\partial \mu}{\partial n_B} = \frac{\partial^2 F}{\partial n_B^2} \geq 0. \tag{45}$$

It is then expected that the chemical potential be an increasing function of baryon number; it will flatten only as we go through the coexistence region of a first order phase transition. We see then that we do not really need the free energy to be linear in the baryon number; when the second derivative vanishes we are at the phase boundary.

In Fig. 7 we see that the chemical potential curves for different baryon numbers overlap, at least at the level of the error bars, for temperatures lower than 170 MeV. By the above argument this part of the curve represents the phase boundary and we can use it to plot in Fig. 8 the phase boundary in the (T, μ) plane.

Before we move on, we would like to point out that, although not explicit in the notation we used above, the chemical potential, as defined in Eq. (39), depends also on the volume and the temperature of the system. In the thermodynamic limit the chemical potential, $\bar{\mu}$, depends only on temperature and density:

$$\bar{\mu}(\rho, T) = \lim_{V \to \infty} \mu(\rho V, V, T). \tag{46}$$

It is then more relevant to think of our measured chemical potential as being defined at a given density. At small baryon number there is an ambiguity as to which density to assign to a particular measurement since the chemical potential is defined to be the difference of the free energies at $n_B + 1$ and n_B baryon numbers. For large values of n_B this does not make much of a difference. Most naturally we should think that the measurement is performed at $n_B + \frac{1}{2}$

Chemical potential
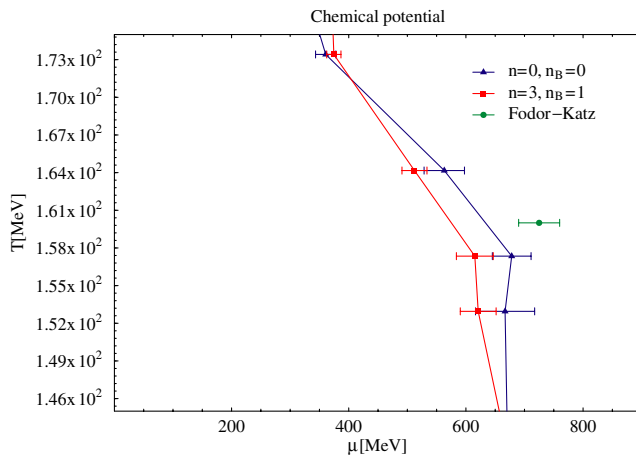
FIG. 8 (color online). Phase transition line based on a model for the free energy. Note that μ is the baryon chemical potential.

and treat $\mu(n_B, V, T)$ as an approximation for $\bar{\mu}(\frac{n_B + \frac{1}{2}}{V}, T)$. For example $\mu(n_B = 0, V, T)$ should be thought as approximating $\bar{\mu}(\frac{1}{2V}, T)$. It is then clear that[1] $\lim_{V \to \infty} \mu(n_B = 0, V, T) = \bar{\mu}(0, T) = 0$, from Eq. (44) which conforms with expectation. But this is not the relevant limit; the limit of interest is that of Eq. (46). In other words the density should be kept fixed when approaching the thermodynamic limit. Note also that using this convention we can show using Eq. (44) that our approximation for the chemical potential becomes symmetric in density, i.e. $\bar{\mu}(-\rho) = -\bar{\mu}(\rho)$.

Another interesting point is that since the chemical potential $\mu(n_B)$ should decrease as the volume is increased (the density decreases) it would seem that the phase boundary constructed using the reasoning we presented above will shift. This is not true: the argument rests on the fact that the chemical potential stays the same as we increase the baryon number; we understand that to be a consequence of the fact that we measure the chemical potential at densities in the phase coexistence region. As we increase the volume, the chemical potential will start to drop only when we get out of the coexistence region but by then it will no longer be independent of n_B. To get back to a chemical potential that is independent of n_B we have to increase the baryon number until the density again is in the coexistence region. Thus the new phase boundary we get at different volumes should be the same (up to finite volume corrections).

C. Quark condensate

As we cross over from the hadronic phase to deconfined phase, we also expect to restore the chiral symmetry. There is ample empirical evidence that the deconfining phase transition and the chiral symmetry restoration occur at almost the same temperatures. As far as we know there is no theoretical explanation of this fact, thus it is interesting to see whether this remains true at finite density. For this purpose, we measure the chiral condensate $\langle \bar{\psi}\psi \rangle$. For fermionic observables, we need not only fold in the phase $\alpha(U)$; we also need to perform a separate Fourier transform. For an arbitrary fermionic bilinear $\bar{\psi}\Gamma\psi$, where Γ is some spinor matrix, we have

$$\langle \bar{\psi}\Gamma\psi \rangle = \frac{1}{\tilde{Z}_C} \frac{1}{N} \sum_{j=0}^{N-1} e^{-in\phi_j} \int \mathcal{D}U e^{-S_g(U)}$$

$$\times \int \mathcal{D}\bar{\psi}\mathcal{D}\psi e^{-S_f(U_{\phi_j}, \bar{\psi}, \psi)} \bar{\psi}\Gamma\psi$$

$$= \left\langle \sum_{n'=0}^{N-1} \frac{\widetilde{\det}_{n'} M^2}{\widetilde{\det}_n M^2} (-2\text{Tr}_{n-n'} \Gamma M^{-1}) \right\rangle, \tag{47}$$

where the factor of 2 comes from using two degenerate

---

[1]We thank F. Karsch for pointing this out and P. de Forcand for an interesting discussion on this point.
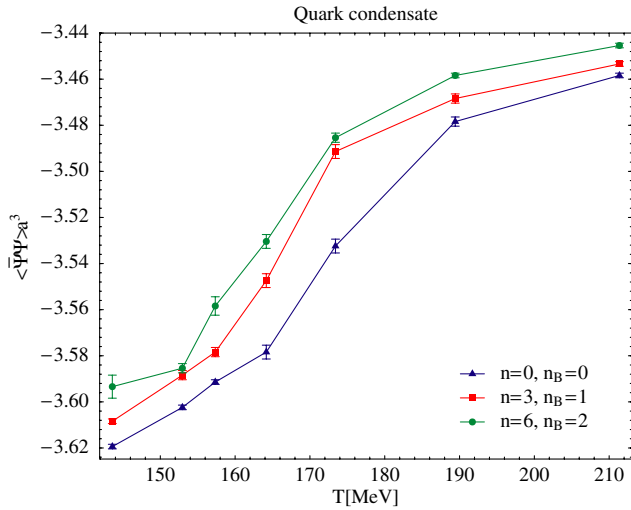
FIG. 9 (color online). The quark condensate $\langle\bar{\psi}\psi\rangle$ in lattice units as a function of temperature.

flavors and we defined

$$\text{Tr}_n\Gamma M^{-1} \equiv \frac{1}{N}\sum_{j=0}^{N-1} e^{-in\phi_j}\,\text{Tr}\Gamma M(U_{\phi_j})^{-1}, \qquad (48)$$

the nth Fourier component of the trace. Note that when computing a fermionic observable, we have contributions not only from the 0th component $\widetilde{\det}_n M^2\,\text{Tr}_0\Gamma M^{-1}$, but also from the parts of the propagator that wrap around the lattice in the time direction. More importantly, determinant sectors other than $\widetilde{\det}_n M^2$ become relevant.

To look for the chiral restoration phase transition, we measure the chiral condensate

$$\langle\bar{\psi}\psi\rangle \equiv \frac{1}{N_f}\frac{2\kappa}{N_4}\sum_x\langle\bar{\psi}(x)\psi(x)\rangle, \qquad (49)$$

where $N_f = 2$ is the number of flavors and N_4 is the lattice four volume. In Fig. 9, we plot the quark condensate as measured in our simulations. We note that as we go through the phase transition, the quark condensate gets smaller. The slope changes in the proper temperature range and the transition temperature seem to decrease with increasing baryon number. Unfortunately, it is not easy to attach much meaning here, since with Wilson fermions the chiral symmetry is broken by lattice artifacts and the quark condensate receives large contributions from these artifacts. Also, the quark mass we employed is very large so the explicit breaking of the chiral symmetry is probably large enough to prevent one from seeing any signal in the chiral condensate.

D. Conserved charge

Finally, we turn our attention to the conserved charge. While in the grand canonical ensemble measuring the

conserved charge,

$$Q(t) = -\kappa\sum_{\vec{x}}[\bar{\psi}(x)U_4(x)(1-\gamma_4)\psi(x+\hat{t})$$
$$-\bar{\psi}(x+\hat{t})U_4^\dagger(x)(1+\gamma_4)\psi(x)], \qquad (50)$$

helps in measuring the average number of particles in the box, there seems to be little point in measuring the conserved charge in the canonical ensemble. In fact, we can prove that if you are to use the true partition function Z_C given in Eq. (11), the charge should be equal to the number of fermions that we put in the box, configuration by configuration. However, since we are simulating an approximation of the partition function, $\tilde{Z}_C$, we can use the conserved charge to check whether our assumption that $\tilde{Z}_C \approx Z_C$ is true. It is easy to show that

$$\langle Q(t)\rangle_{\tilde{Z}_C(n)} = \frac{\sum_m(n+mN)Z_C(n+mN)}{\sum_m Z_C(n+mN)}. \qquad (51)$$

We see then that the deviation from the expected number of quarks would quantify how much mixing of different quark sectors we have.

In our simulations, we used $N = 12$ and $n = 0, 3$ and 6. For the $n = 0$ and $n = 6$ simulations, we can prove that the conserved charge will be zero. In the $n = 0$ case, this is due to the charge conjugation symmetry $Z_C(n) = Z_C(-n)$. For the $n = 6$ simulation, this is due to the fact that for every number of the form $6 + 12m$ there is another integer m' such that $6 + 12m' = -(6 + 12m)$; plugging this in the expression above we get $\langle Q\rangle_{n=6} = 0$. The only nontrivial case is when $n = 3$, which we plotted in Fig. 10. We see that as the quarks become deconfined, the chemical potential drops and the mixing with the other sectors becomes more important. However, even for large temperatures,
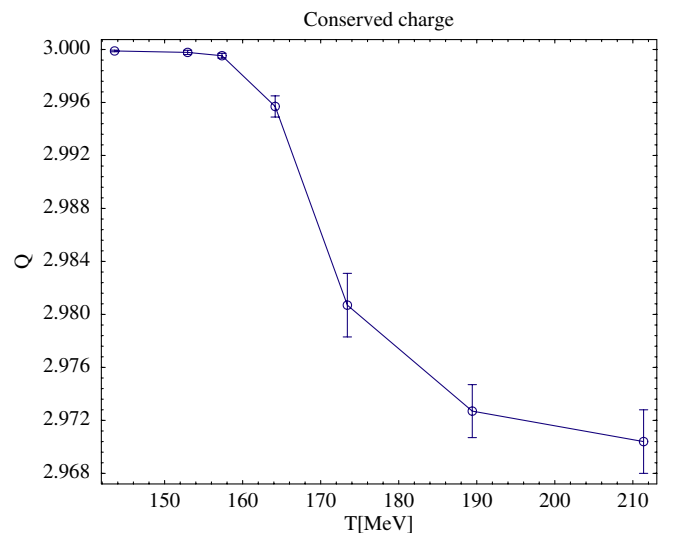
FIG. 10 (color online). Total number of particles in the box for the $n = 3$ simulations as a function of temperature.

$T \sim 200$ MeV, the mixing is only about 1%. This implies that even the nearest sector, $Z_C(n = 9)$, is greatly suppressed, i.e. $Z_C(n = 9)/Z_C(n = 3) \sim 0.01$. The mixing is small mainly because the chemical potential is large; the mixing will get worse when we decrease the fermion mass.

In conclusion, in this section we show that we can see the expected deconfining transition in the Polyakov loop, that the chemical potential drops as we go from the hadronic phase to the quark-gluon plasma phase, and that there is some hint of the transition even in the chiral condensate. Using the conserved charge, we have checked that the approximation we made, employing a discrete Fourier transform rather than a continuous one, is valid.

VI. CONCLUSIONS AND OUTLOOK

In this paper, we show that the canonical partition function can be used to investigate the phase structure of QCD at finite temperature and nonzero density. The algorithm we employed allows us to investigate densities much higher than the nuclear matter density, at least for the parameters used in the present study. Sign fluctuations limit our ability to reach very low temperatures or much larger densities than the ones explored here. We also checked that the discrete Fourier approximation to the canonical partition function introduces only minimal deviations.

The physical picture that emerges from our simulations is consistent with expectations. The Polyakov loop, the chemical potential and the quark condensate show signs of a transition around $T \sim 170$ MeV. The quark condensate does not vanish but we need to employ smaller masses and finer lattices to reasonably expect a clear signal of chiral symmetry restoration. Another route is to employ a more sophisticated definition for the chiral condensate, involving perhaps some form of subtraction, or use chiral fermions.

Before moving on to future plans, we should point out that our goal in this exploratory study has been to determine the feasibility of the canonical partition function approach. Because of practical considerations, we only used 4^4 lattices with $N = 12$. Further studies are needed to address questions related to the volume dependence of our results. Furthermore, while we provided a test of the discrete Fourier approximation, a more convincing way to check our results would be to run our simulations at larger values of N. We plan to address these questions as soon as we implement the determinant estimator.

In the future, we would also like to locate points on the phase transition line. For this, we need to get to lower temperatures and densities. While we might be limited in reaching lower temperatures, we should be able to reach lower densities; all we need is to move to larger volumes. However, since we have to use larger lattices we need to use an estimator for the determinant. We should point out that the method used to generate the ensemble has no bearing on whether we have a sign problem or not, it is an intrinsic property of the ensemble. Consequently, the sign oscillations stay the same even when we employ the determinant estimator. The only thing that is going to change is the acceptance rate. We anticipate that this should not be a problem since the acceptance rate is very good for rather large HMC trajectory lengths. However, this need to be studied further.

Before we conclude, we would like to emphasize that, even if it proves that it is not feasible to reach lower temperatures, this approach is valuable since it permits the study at the phase diagram at temperatures close to T_c and rather large densities. We will then be able to determine various points on the phase transition line. Much effort is put nowadays on determining this line, and as we pointed out in the beginning, the methods used today need to be checked for reliability. To stress this point, we plot in Fig. 8, next to our phase transition line, the second order phase transition point as determined by Fodor and Katz [3]. Their simulations use different quark masses, but the shape of the transition line is expected to change very little. Although our error bars are rather large, the plot suggests the possibility of a discrepancy. This has also been noted in [10] and a possible explanation is provided in [24]. These results seem to indicate a possible overlap problem. It is then imperative that new simulations are carried out to check the validity of this important result. A future study that employs a determinant estimator will allow us to collect better statistics and hopefully will settle this question.

ACKNOWLEDGMENTS

[1] I. M. Barbour, S. E. Morrison, E. G. Klepfish, J. B. Kogut, and M.-P. Lombardo, Nucl. Phys. B, Proc. Suppl. **60**, 220 1998)

[2] P. Crompton, Nucl. Phys. **B619**, 499 (2001).

[3] Z. Fodor and S. D. Katz, J. High Energy Phys. 03 (2002) 014.

[4] Z. Fodor and S. D. Katz, J. High Energy Phys. 04 (2004) 050.

[5] C. R. Allton *et al.*, Phys. Rev. D **68**, 014507 (2003).

[6] C. R. Allton *et al.*, Phys. Rev. D **71**, 054508 (2005).

[7] P. de Forcrand and O. Philipsen, Nucl. Phys. **B642**, 290 (2002).

[8] J. Engels, O. Kaczmarek, F. Karsch, and E. Laerman, Nucl. Phys. **B558**, 307 (1999).

[9] S. Kratochvila and P. de Forcrand, Nucl. Phys. B, Proc. Suppl. **129**, 533 (2004).

[10] S. Kratochvila and P. de Forcrand, Nucl. Phys. B, Proc. Suppl. **140**, 514 (2005).

[11] K. F. Liu, Int. J. Mod. Phys. B **16**, 2017 (2002).

[12] K. F. Liu, *QCD and Numerical Analysis* Vol. III (Springer, New York, 2005), p. 101.

[13] A. Alexandru, M. Faber, I. Horváth, and K. F. Liu, Nucl. Phys. B, Proc. Suppl. **140**, 517 (2005).

[14] P. Hasenfratz and F. Karsch, Phys. Lett. B**125**, 308 (1983).

[15] B. Joo, I. Horváth, and K. F. Liu, Phys. Rev. D **67**, 074505 (2003).

[16] A. Alexandru and A. Hasenfratz, Phys. Rev. D **66**, 094502 (2002).

[17] M. Faber, O. Borisenko, S. Mashkevich, and G. Zinovev, Nucl. Phys. **B42**, 484 (1995).

[18] A. Roberge and N. Weiss, Nucl. Phys. **B275**, 734 (1986).

[19] C. Thron, S. J. Dong, K. F. Liu, and H. P. Ying, Phys. Rev. D **57**, 1642 (1998).

[20] R. Sommer, Nucl. Phys. **B411**, 839 (1994).

[21] S. Gottlieb, W. Liu, D. Toussaint, R. L. Renken, and R. L. Sugar, Phys. Rev. D **35**, 2531 (1987).

[22] S. Duane, A. D. Kennedy, B. J. Pendleton, and D. Roweth, Phys. Lett. B **195**, 216 (1987).

[23] S. Ejiri, Phys. Rev. D **69**, 094506 (2004).

[24] K. Splittorff, hep-lat/0505001.